processes

MDPI

Article

The Influence of Nitrogen Absorption on Microstructure, Properties and Cytotoxicity Assessment of 316L Stainless Steel Alloy Reinforced with Boron and Niobium

Sadaqat Ali [1,2,*], Ahmad Majdi Abdul Rani [1,*], Riaz Ahmad Mufti [2], Farooq I. Azam [2], Sri Hastuty [3], Zeeshan Baig [4], Murid Hussain [5] and Nasir Shehzad [5]

1 Mechanical Engineering Department, Universiti Teknologi PETRONAS (UTP), Bandar Seri Iskandar, Perak Darul Ridzuan 32610, Malaysia
2 School of Mechanical & Manufacturing Engineering, National University of Sciences and Technology (NUST), H-12, Islamabad 44000, Pakistan
3 Mechanical Engineering Department, Universitas PERTAMINA, Jakarta 12220, Indonesia
4 Centre of Excellence in Science & Applied Technologies, Islamabad 44000, Pakistan
5 Department of Chemical Engineering, COMSATS University Islamabad, Lahore Campus, Defense Road, Off Raiwind Road, Lahore 54000, Pakistan
* Correspondence: engineersadaqat@gmail.com (S.A.); majdi@utp.edu.my (A.M.A.R.); Tel.: +92-333-9410290 (S.A.); +60-5368-7155 (A.M.A.R.)

Received: 23 June 2019; Accepted: 19 July 2019; Published: 2 August 2019

Abstract: In the past, 316L stainless steel (SS) has been the material of choice for implant manufacturing. However, the leaching of nickel ions from the SS matrix limits its usefulness as an implant material. In this study, an efficient approach for controlling the leaching of ions and improving its properties is presented. The composition of SS was modified with the addition of boron and niobium, which was followed by sintering in nitrogen atmosphere for 8 h. The X-ray diffraction (XRD) results showed the formation of strong nitrides, indicating the diffusion of nitrogen into the SS matrix. The X-ray photoelectron spectroscopy (XPS) analysis revealed that a nitride layer was deposited on the sample surface, thereby helping to control the leaching of metal ions. The corrosion resistance of the alloy systems in artificial saliva solution indicated minimal weight loss, indicating improved corrosion resistance. The cytotoxicity assessment of the alloy system showed that the developed modified stainless steel alloys are compatible with living cells and can be used as implant materials.

Keywords: implant; stainless steel; nickel; leaching; nitrogen; cytotoxicity

1. Introduction

Biomedical implants and devices are critical to enhancing the quality of life, and the nature and life span of human beings [1]. The restoration of parts of the human body using implants is an ancient field and dates back 4000 years ago when gold and iron was used for dental applications by Egyptians and Romans [2]. The advancement in producing biomedical implants is closely related to the development of biomaterials with tailored mechanical properties. This field has gained substantial attention over the last few decades, and since the first summit on the development of biomaterials was held in 1969 [3]. Since then, there has been continuous effort to develop new materials and improve the existing manufacturing methods for the betterment of humankind in terms of implantation devices. A suitable choice of biomedical material for implant manufacturing is very crucial for its long term success, and should include consideration of its wear resistance, biocompatibility, corrosion resistance, mechanical properties, economics and ease of manufacturing [4,5].

Among the various biomaterials available, austenitic 316L stainless steel has been in use since the 1930s, when it was utilized in the total hip replacement of an orthopaedic patient [6,7]. Since then, it has gained tremendous attention as a biomaterial for implant manufacturing owing to its biocompatibility, adequate mechanical properties, ease of manufacturing, decent corrosion resistance, and cheaper cost [8,9]. ASTM International also recommends the 316L type amongst the various available grades of austenitic stainless steels for its usage as an implant material. The high concentration of chromium and low carbon content improves its tendency towards chlorine bearing solutions as far as corrosion resistance is concerned [10,11]. Saline in the human body has a close resemblance to chlorine-bearing solutions and this makes 316L SS an ideal material for the human body [12]. However, there are some problems associated with the use of this medical grade alloy [13]. Several studies on retrieved 316L SS implants from patients have revealed that 90% of the implant failures were due to corrosion attacks due to pitting [14,15]. One of the most important aspects in this regard is the leaching of nickel ions from the SS matrix [13,16,17]. The release of nickel and other metal ions from implants are clearly associated with poor corrosion resistance in humans [18–22]. The leaching of metal ions and poor corrosion resistance necessitates the modification of the 316L SS matrix by alloying it with additives and improving the surface layer of the implants [23–25].

To extend the applicability of SS as an implant material, the addition of niobium in the SS matrix can help to increase the corrosion resistance of the resulting modified SS alloy. In the last few decades, niobium has attracted much attention for its potential use as a biomaterial [26–28]. Niobium has proved to be an important and promising alloying element [29] with adequate biocompatibility for biomedical applications [30,31]. It exhibits good corrosion resistance and strength for its potential use in implant applications [32,33]. Boron has proved to be a promising additive to increase the densification process [34,35] and for increasing the overall density of the resulting stainless steel alloy [36]. Both these alloying elements address the highlighted issues related to the use of SS alloy as an implant material. Sintering of SS alloy in nitrogen has been proven to improve the densification process as well as improving the mechanical properties [37]. In this study, sintering of the alloy was carried out in nitrogen atmosphere for 8 h to develop a nitride layer on the surface of the alloy.

2. Materials and Methods

In this study, gas atomized 316L SS powder was used as the matrix to prepare the samples. The amount of boron addition was limited to 0.25 wt.% for activated sintering for maximum densification, as per our previous studies [9,34,38] whereas the amount of niobium was varied from 0.5 wt.% to 2 wt.%. The SEM images and XRD analysis of all the powders used in the study are shown in Figures 1 and 2, respectively. The XRD spectrum clearly indicates the presence of chromium, iron and nickel in the stainless steel powder at their respective peaks, along with boron and niobium peaks in their respective spectrum as shown in Figure 2.

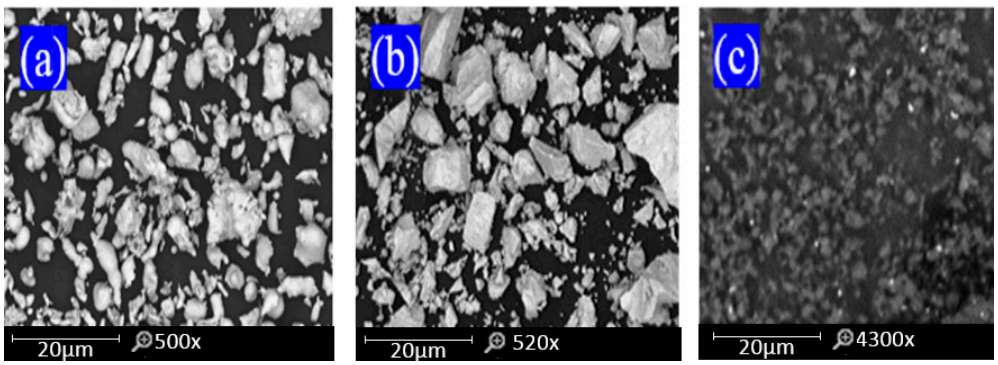

Figure 1. SEM images of (**a**) 316L SS, (**b**) niobium, and (**c**) boron powder.

A total of five composites were made in this study. These were named as S1 (pure 316L SS); S2 (316L SS + 0.25 B + 0.5 Nb); S3 (316L SS + 0.25 B + 1 Nb); S4 (316L SS + 0.25 B + 1.5 Nb); and S5 (316L SS + 0.25 B + 2 Nb). Each powder composition was prepared by blending the respective amount of each powder in a tubular mixer for 8 h. The powder from each mixture was compacted into a disc shape of 30 mm diameter and ~4 mm thick using the uniaxial cold compaction process at a pressure of 800 MPa. The compacted samples were then sintered in a tube furnace (Model: Protherm, PTF12/75/800, Alserteknik, Ankara, Turkey). Nitrogen was selected as the sintering atmosphere and a temperature of 1200 °C was used for sintering all of the samples. The dwell time was kept at 8 h for maximum absorption of nitrogen into the samples.

The green densities of the samples were calculated using geometric method, whereby the diameter and thickness of the compacted samples was measured. The green density was then calculated by dividing the mass of the sample by its volume as given by Equation (1).

$$Green\ density = \frac{Mass}{Volume} \quad (1)$$

The sintered densities for all the samples were measured using Archimedes' principle. The HR-150 AZ analytical balance manufactured by A&D Company, Limited, Tokyo, Japan was used for the density measurement. Three samples of each formulation were measured and the average value of sintered density was recorded. The relative density of each sample were calculated by dividing the sintered density by the theoretical density of pure 316L stainless steel as the reference, as shown by Equation (2). The standard deviation of green and sintered densities for all the samples were calculated and are given in Table 1.

$$Relative\ density = \frac{\rho_{experimental}}{\rho_{theoretical}} \quad (2)$$

The optical microscope (Model: Leica DM LM, Wetzlar, Germany) was used to examine the microstructure after being properly etched. The Carpenters stainless steel etchant solution was used to etch the samples, which were composed of 8.5 g Ferric Chloride ($FeCl_3$), 2.4 g Cupric Chloride ($CuCl_2$), 122 mL Hydrochloric acid (HCl), 6 mL Nitric acid (HNO_3) and 122 mL Ethanol. The samples were immersed in the solution for 30 s before being observed in the microscope.

The microhardness of the sintered samples was calculated via Vickers hardness tester (Model: Leco LM 247AT, St Joseph, MI, USA) by applying 200 gf and 15 s dwell time. At least five values were recorded for each sample from different locations and the average value was calculated.

The XRD analysis of the samples was done using the X-ray diffractometer (Model: X'pert3, Powder and Empyrean, PANalytical, B.V, Lelyweg, Almelo, The Netherlands) for the presence of possible compounds using the 10–100° scan range. The XRD peaks were then indexed and identified using High Score Plus software.

The XPS analysis was done using an X-ray photoelectron spectrometer (Model: Thermo scientific, K-alpha, East Grinstead, UK) for the analysis of elemental mass percentages of different elements on the sample surface. The XPS analysis shows all the elements that are present within the film and those bonded to it. It can be used to detect the foreign elements that might be present on the sintered sample surface. Since XPS can observe surface of nm order, the nitrogen and other elements present on the sample surface were detected by this method.

The corrosion resistance of the developed compositions was found by the weight loss method, whereby the samples were immersed in artificial saliva solution. The artificial saliva used in the testing had a composition of urea (1.0 g/L), KCl (0.4 g/L), NaCl (0.4 g/L), $Na_2S{\cdot}9H_2O$ (0.005 g/L), $NaH_2PO_4{\cdot}H_2O$ (0.69 g/L) and $CaCl_2{\cdot}2H_2O$ (0.795 g/L) with a pH of 5.5 to adjust it to the composition of natural saliva [39,40]. All the samples were first weighed and then immersed in the solution for 28 days. After a period of 28 days, each sample was cleaned and weighed again to calculate the change in weight incurred during this time period.

For the cytotoxicity testing of the samples, cell cultures were done using fibroblast cell line on all the samples. The fibroblast cell line (NIH/3T3 ATCC® CRL-1658) supplied by ATCC, Manassas, VA, USA were expanded in the media, using Dulbecco's Modified Eagle's Medium (DMEM) supplied by ThermoFisher Scientific, Waltham, MA, USA. It involved 100 µg/mL of Pen/strep (Sigma Aldrich, Life Sciences, Saint Louis, MO, USA) supplemented by 10 percent foetal bovine serum (FBS) (Sigma Aldrich, Life Sciences, USA). NIH/3T3 cells were expanded in a T75 culture flask (Corning Biosystem) at a temperature of 37 °C, and grown to 90% confluency with fresh media changes after 2 to 3 days in an incubator with 5% CO_2. After this, the cells were detached using trypsin–EDTA (Sigma Aldrich, Life Sciences, USA). On seeding day, the cells were counted with a haematocytometer and microscope. Fifty thousand cells were seeded on each sample in the 6-well plate to check the compatibility of the NIH/3T3 cells with the samples. Before seeding, the samples were diluted by adding 100 µL of the sample DMEM media into 1 mL. The cells were cultured on tissue culture plastic plates without samples, to use as control to compare the values with the cells cultured in the presence of DES samples. Before seeding of the cells, the samples were sterilized with ethanol solution for one hour and rinsed with phosphate buffer saline (PBS) for 15 min. The cells that were cultured without the samples were used as the controls. The fluorescent measurements of Alamar Blue were taken after three days to quantify the cells. The cell seeded samples were rinsed with PBS solution. They were then kept for incubation at 37 °C. Using a fluorescence plate reader (Bio-TEK, NorthStar Scientific Ltd., Bedfordshire, UK), 3–4 h absorbance was calculated at 570 nm. The cell metabolic activity took place and incorporated an oxidation-reduction indicator that changes colour as well as fluoresces. This was in response to chemical reduction that took place due to cell growth. The REDOX indicator changed colour from blue (oxidized) to red (reduced) due to growth.

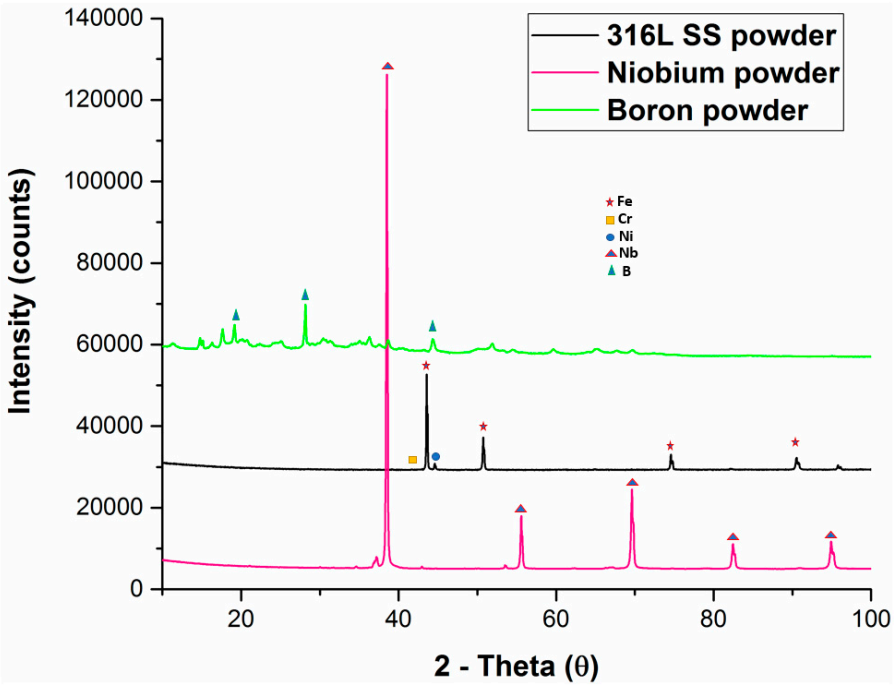

Figure 2. XRD spectra of niobium, boron and 316L SS powder.

3. Results and Discussion

The green and sintered densities of the samples that were produced are depicted in Table 1. The green density of pure 316L SS was found to be 6.5 g/cm^3. There is a slight decrease in the green density of the boron and niobium added SS samples. This is due to the fact that the boron and niobium particles tried to induce themselves in the matrix of SS. Sintering in nitrogen atmosphere resulted in improved sintered density for all the samples. Results of the sintered density show that the sintering environment

and temperature promoted adequate densification. The pure 316L SS achieved a maximum sintered density of 7.575 g/cm^3. The density for boron and niobium added samples resulted in a slight decrease in sintered density. The amount of additive had a noticeable effect on the resulting properties of the alloy system. The boron addition improved the densification process and helped to maintain the density near to the sintered density of pure SS samples. Although there is a slight reduction in the sintered density of the samples with niobium and boron, their impact on the hardness, corrosion resistance and cytotoxicity were noticeable. From the analysis, the standard deviation values for green and sintered densities were within the permissible limits. This shows that the results have good repeatability.

Table 1. Densities of all the samples.

Alloy	Green Density	Standard Deviation	Sintered Density	Standard Deviation	Relative Density
S1	6.500 g/cm^3	0.112	7.575 g/cm^3	0.063	95.88%
S2	6.370 g/cm^3	0.0432	7.411 g/cm^3	0.023	93.81%
S3	6.240 g/cm^3	0.057	7.367 g/cm^3	0.051	93.25%
S4	6.160 g/cm^3	0.035	7.285 g/cm^3	0.092	92.21%
S5	6.080 g/cm^3	0.029	7.190 g/cm^3	0.028	91.01%

The microstructure of 316L samples with and without the addition of additives was observed using an optical microscope as shown in Figure 3. The sintering temperature and environment resulted in almost fully dense samples. It is evident from Figure 3 that all the samples were sintered properly with significantly low porosity. There were voids present in each sample showing that there is a very little porosity present in the samples. The nitrogen diffused into the matrix and formed strong nitrides with iron, boron and niobium. This resulted in increased microhardness of the samples and was also helpful in controlling the leaching of ions.

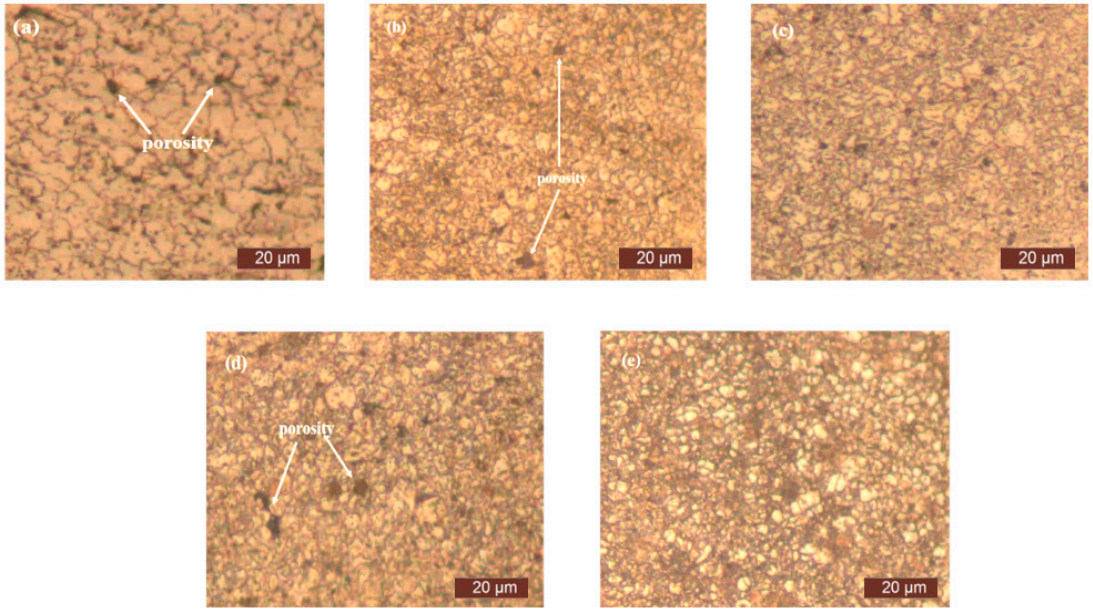

Figure 3. Microstructure of sintered samples (**a**) S1 (**b**) S2 (**c**) S3 (**d**) S4 (**e**) S5.

The porosity in the sintered samples was calculated from the sintered density (ρ_a) and the theoretical density (ρ_{th}) of the alloy using the formula shown in Equation (3) as per the literature [41,42].

$$Porosity = 1 - \frac{\rho_a}{\rho_{th}} \quad (3)$$

The estimation of the pores present in the sintered samples is presented in Table 2. The results indicate that nearly all the samples have less porosity. The porosity increased with increased amounts of added titanium. The lowest porosity was observed in the pure 316L stainless steel sintered samples and this increased to 8.60 for the 2 wt.% titanium added samples.

Table 2. Porosity estimation of sintered samples.

Sample	S1	S2	S3	S4	S5
Porosity (%)	4.10	5.68	6.20	7.36	8.60

The micro hardness of the samples indicated an upsurge in micro hardness due to the infusion of nitrogen into the matrix. A micro hardness value of 235 HV was observed for 316L SS samples. The addition of boron has also had a significant role in increasing the micro hardness. The addition of niobium also increased the micro hardness of the sintered samples. The quantity of niobium addition also had an effect on the micro hardness and it increased with an increase in the quantity of niobium. A maximum of 387 HV was observed for samples with the addition of 2 wt.% niobium. The hardness of all the samples is shown in Figure 4.

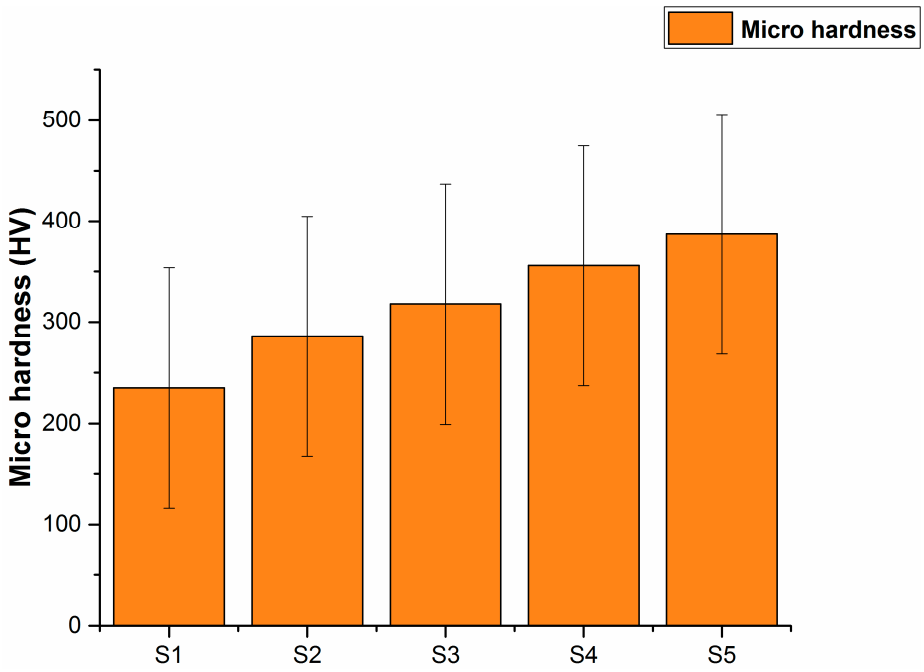

Figure 4. Micro hardness of all samples.

XRD analysis of all the sintered samples was done in order to analyse the different compounds formed during sintering of the samples. Figure 5 illustrates the XRD patterns of all the samples studied in this research. The results show the presence of austenitic structure in all the samples and ɣFe is also present in all the samples. The XRD patterns for pure 316L SS samples and boron and niobium added samples clearly reveal the diffusion of nitrogen into the matrix and the formation of strong nitrides. The patterns of pure 316L SS samples show the formation of $FeN_{0.324}$ at d spacing of 2.07500, C_3N_4 at d spacing of 2.51960, Ni (Cr_2O_4) at d spacing of 2.49354, and Cr_2O_3 at d spacing of 2.66348. These compounds clearly show the presence of nitrogen in the stainless steel matrix, forming nitrides with iron and carbon. For the samples of 0.5 wt.% niobium, the presence of $B_{0.47}C_{0.23}N_4$ at d spacing of 3.33850, Cr_2O_3 at d spacing of 2.66591, $B_2Fe_3Ni_3$ at d spacing of 2.07846, and NbB_2 at d spacing of 2.07838 was observed. The boron present in the matrix made a complex compound with carbon in the matrix and the diffused nitrogen. Moreover, the nitrogen also formed compounds with iron

present in the SS matrix. The XRD results for 1 wt.% niobium added samples indicated the presence of $Cr_{1.3}Fe_{0.7}O_3$ at d spacing of 2.67600, $Nb_{0.76}B_2$ at d spacing of 2.08500, $FeN_{0.0499}$ at d spacing of 2.08019, and Fe_2O_3 at d spacing of 1.68000. In 1.5 wt.% niobium added samples, the following compounds were noted: B_2CN at d spacing of 2.13164, Cr_2O_3 at d spacing of 2.66439, $FeN_{0.0560}$ at d spacing of 2.08366, and $NbN_{0.9}$ at d spacing of 2.52706. The identified compounds for 2 wt.% niobium added SS samples were B_2CN at d spacing of 2.13164, $FeN_{0.0560}$ at d spacing of 2.08366, and $Cr_{1.3}Fe_{0.7}O_3$ at d spacing of 2.67600. These results indicate the formation of strong nitrides and borides that are responsible for the improvement of mechanical properties, including the hardness of the produced samples. The formation of chromium oxides favoured the creation of a passive surface oxide layer on the sample's surface. These results are similar to the results reported for the oxidation of metal surfaces [43]. These oxide layers thus increase the corrosion resistance of the produced samples.

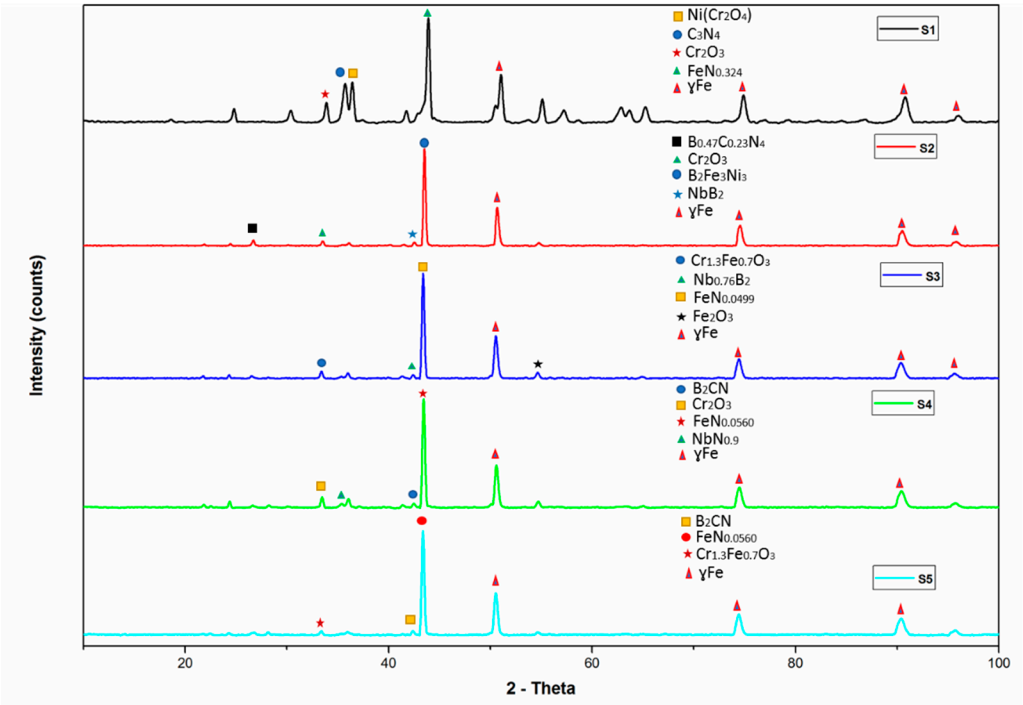

Figure 5. XRD spectra of all sintered samples.

XPS analysis was done to find the different elements present on the produced samples' surfaces. The X-ray photoelectron spectroscopy (XPS) is a quantitative surface-sensitive technique that plays an important role in determining the surface chemistry and elemental composition of a material. It involves the use of X-rays to radiate a material. The kinetic energy is measured while the number of escaped electrons is recorded. The XPS shows all the elements that are in the film and those bonded to it. It can be used to detect foreign elements that might be present on the sintered sample surface. The XPS analysis for all sintered samples is shown in Figure 6. The results indicate the presence of iron, chromium, oxygen and nitrogen, which constitute the main elements present on the sample surface. The sintered samples were covered with thin nano-size passive film consisting of chromium and iron oxide along with nitrogen. From the analysis, the amount of nitrogen present on the surface of the samples varied from 2.82% to a maximum of 3.9%. The maximum amount was observed for 2 wt.% niobium added stainless steel samples. The analysis indicated that the sintering parameters allowed the formation of a strong nitride layer along with chromium and iron oxide layers on the sintered samples. These layers serve as a coating for the samples by not allowing foreign bodies to diffuse into the matrix and they also control the leaching of ions. The presence of chromium and iron indicate the formation of surface oxide films on the surface of the sintered samples. These surface oxide films play a vital role in controlling the leaching of ions by acting as an inhibitor [44].

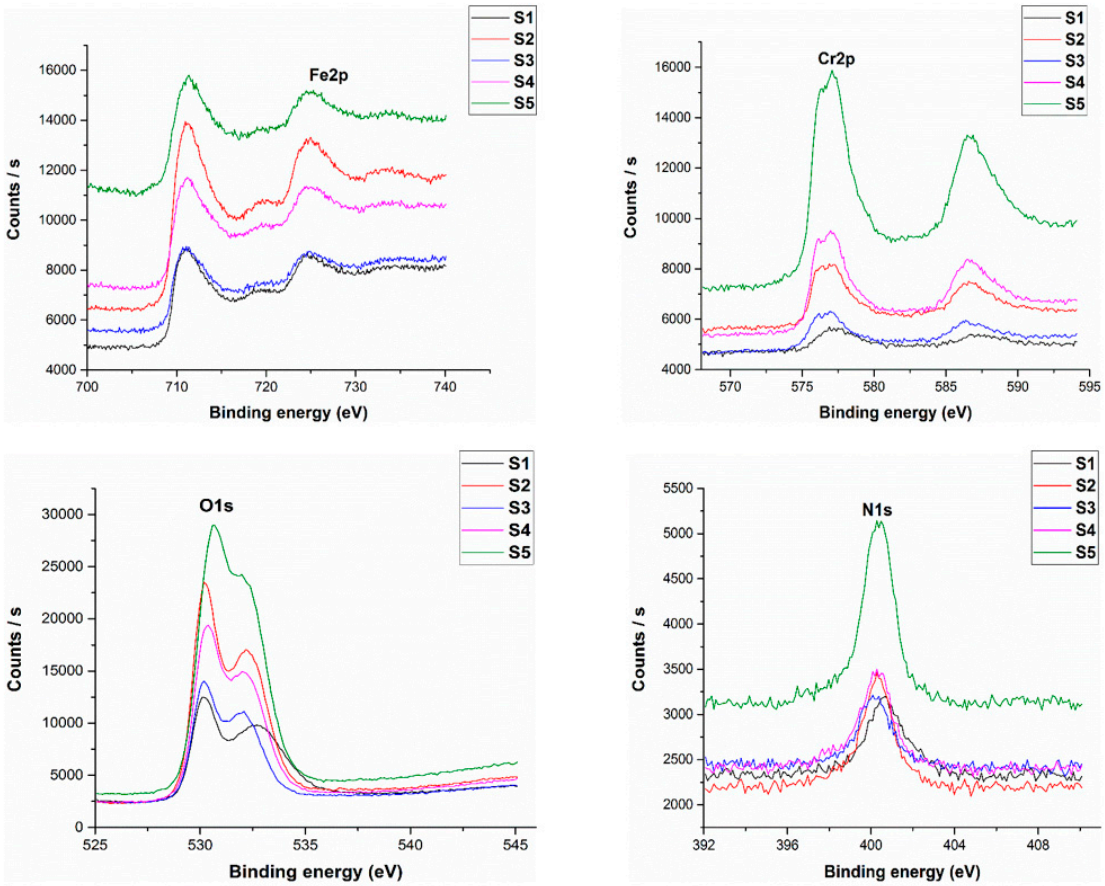

Figure 6. XPS spectra for Fe2p, Cr2p, O1s and N1s of all sintered samples.

To investigate the outcome of the alloying elements and sintering parameters, we estimated the corrosion resistance of the developed samples. The samples were cleaned and put into an artificial saliva solution and the resulting behaviour was studied. After immersing the samples in artificial saliva solution for 28 days, the minimal weight loss was observed. The weight loss measurements for all the samples are tabulated in Table 3. The results shows that the developed materials have a very good corrosion resistance to the artificial saliva solution. The pure 316L stainless steel samples showed a maximum weight loss of 0.003 g whereas the 1, 1.5 and 2 wt.% niobium added stainless steel samples showed an equal reduction in weight, even after 28 days of immersion. This indicates that these three samples were stable against the attack of solution ions. The samples showed more resistance towards corrosion compared to samples S1 and S2. The reduced weight loss also corresponds to the fact that the nitride layer along with the surface oxide layer was strong enough to retain itself throughout the process. This also relates to the fact that these layers retained the nickel and other ions present in the matrix. The proposed strategy of nitriding the surface layer proved to be efficient for the retention of nickel and other metal ions.

Table 3. Weight loss measurements for all samples in artificial saliva solution.

S.No	Sample	Weight (g) before Immersion	Weight (g) after Immersion	Δ m (g)
1	S1	17.310	17.306	0.004
2	S2	18.130	18.127	0.003
3	S3	18.190	18.188	0.002
4	S4	17.260	18.258	0.002
5	S5	18.250	18.248	0.002

In vitro cytotoxicity assessment of each of the membrane was determined by culturing NIH3T3 ATCC® CRL-1658 (fibroblast cell line) on the samples. Alamar Blue Assay was utilized to assess the cell proliferation on day 3. Microplate reader absorbance graph analysis was done to assess the cell viability of the liquid chemicals. The experiment was performed for 3 days by co-culturing with liquids and the results were then compared with the control. Figure 7 shows the comparison of the results of the control for 3 days with the results of the deep eutectic solvents for 3 days. The proliferation increased with time, i.e., up to 3 days for deep eutectic solvents which was also in contrast to the control. The increase in the absorbance rate indicates the increase of cell proliferation. All the samples showed increased absorbance as compared to the control. Sample S5 containing 2 wt.% niobium added stainless steel samples showed the best results as it shows more antibacterial properties which indicates the highest cell proliferation. The corrosion resistance of samples S3, S4 and S5 indicated that they were equally resistant to the artificial saliva solution attack and all of them showed the same weight loss. However, in terms of cytotoxicity assessment, the cell proliferation of S4 was the lowest amongst the three. The absorbance of S3 was better than S4 but less than S5. These results indicate that the material composition has a notable effect as far as the cytotoxicity assessment is concerned. From the figure, it can be noticed that all the produced samples are non-cytotoxic and compatible to living cells. All the analysis was conducted at least twice, with five readings from each of the experimental samples in order to obtain precise data. Sample S5 had the maximum increase in cell proliferation as compared to the control as well as to the other samples. This test also supports the argument for using these composites for biomedical application.

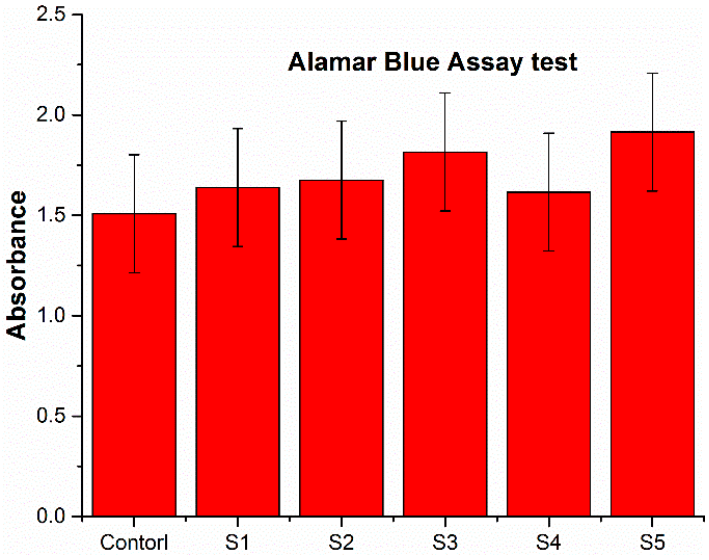

Figure 7. Cytotoxicity assessment of all the samples.

4. Conclusions

The nitrogen atmosphere for sintering austenitic stainless steel favoured the development of a strong nitride layer on the surface of the samples. An amount of 3.9% of nitrogen was found for those samples with an addition of 2 wt.% niobium. The dwell time of 8 h helped the diffusion of nitrogen into the matrix and formed strong nitrides with iron, carbon and other elements present in the stainless steel. The amount of the niobium addition was limited to 2 wt.% and this helped in the retention of the austenitic structure of the stainless steel. The samples were properly sintered at these sintering parameters and showed almost fully dense microstructures. The porosity of the samples was well within the limits and had minimal effect on the properties of the alloy systems. The 1, 1.5 and 2 wt.% niobium added samples showed maximum resistance to corrosion and had minimal weight loss. However, the cytotoxicity assessment of S5 was better compared to other samples studied in this

research. All the sample compositions studied in this research are compatible with living tissues and are well suited to be used in biomedical implant manufacturing.

Author Contributions: Conceptualization, S.A.; Formal analysis, S.A.; Funding acquisition, R.A.M. and A.M.A.R.; Methodology, S.A.; Project administration, A.M.A.R. and R.A.M.; Resources, S.H., M.H. and N.S.; Supervision, A.M.A.R. and R.A.M.; Writing—original draft, S.A.; Writing—review & editing, Z.B. and F.I.A.

Funding: This research was funded by Universitas PERTAMINA—Universiti Teknologi PETRONAS (UP-UTP) International Collaborative Research Fund, cost-centers 015LB0-040 and 015ME0-081 and The APC was funded by Universiti Teknologi PETRONAS, Malaysia and National University of Sciences and Technology (NUST), Islamabad, Pakistan.

Acknowledgments: The authors would like to acknowledge Universiti Teknologi PETRONAS, Malaysia for carrying out research and other facilities.

Conflicts of Interest: The authors declare no conflict of interest.

References

1. Kang, C.-W.; Fang, F.-Z. State of the art of bioimplants manufacturing: Part I. *Adv. Manuf.* **2018**, *6*, 20–40. [CrossRef]
2. Manivasagam, G.; Dhinasekaran, D.; Rajamanickam, A. Biomedical implants: Corrosion and its prevention-a review. *Recent Patents Corros. Sci.* **2010**. [CrossRef]
3. Geetha, M.; Singh, A.K.; Asokamani, R.; Gogia, A.K. Ti based biomaterials, the ultimate choice for orthopaedic implants—A review. *Prog. Mater. Sci.* **2009**, *54*, 397–425. [CrossRef]
4. Kang, C.-W.; Fang, F.-Z. State of the art of bioimplants manufacturing: Part II. *Adv. Manuf.* **2018**, *6*, 137–154. [CrossRef]
5. Dwivedi, C.; Pandey, H.; Pandey, A.C.; Patil, S.; Ramteke, P.W.; Laux, P.; Singh, A.V. In Vivo Biocompatibility of Electrospun Biodegradable Dual Carrier (Antibiotic+ Growth Factor) in a Mouse Model—Implications for Rapid Wound Healing. *Pharmaceutics* **2019**, *11*, 180. [CrossRef]
6. Wiles, P. The surgery of the osteo-arthritic hip. *Br. J. Surg.* **1958**, *45*, 488–497. [CrossRef]
7. Wiles, P. The classic: The surgery of the osteo-arthritic hip. *Clin. Orthop. Relat. Res.* **2003**, *417*, 3–16.
8. Lo, K.H.; Shek, C.H.; Lai, J. Recent developments in stainless steels. *Mater. Sci. Eng. R Rep.* **2009**, *65*, 39–104. [CrossRef]
9. Ali, S.; Rani, A.M.A.; Altaf, K.; Baig, Z. Investigation of Boron addition and compaction pressure on the compactibility, densification and microhardness of 316L Stainless Steel. In *IOP Conference Series: Materials Science and Engineering*; IOP Publishing: Bristol, UK, 2018.
10. Park, J.B. *Biomaterials Science and Engineering*; Springer Science & Business Media: Berlin, Germany, 2012.
11. Khuenkaew, T.; Kanlayasiri, K. Resistance Spot Welding of SUS316L Austenitic/SUS425 Ferritic Stainless Steels: Weldment Characteristics, Mechanical Properties, Phase Transformation and Solidification. *Metals* **2019**, *9*, 710. [CrossRef]
12. Saini, M.; Singh, Y.; Arora, P.; Arora, V.; Jain, K. Implant. biomaterials: A comprehensive review. *World J. Clin. Cases WJCC* **2015**, *3*, 52. [CrossRef]
13. Salahinejad, E.; Hadianfard, M.J.; Macdonald, D.D.; Sharifi-Asl, S.; Mozafari, M.; Walker, K.J.; Rad, A.T.; Madihally, S.V.; Tayebi, L. In vitro electrochemical corrosion and cell viability studies on nickel-free stainless steel orthopedic implants. *PLoS ONE* **2013**, *8*, e61633. [CrossRef]
14. Sivakumar, M.; Kumar Dhanadurai, K.S.; Rajeswari, S.; Thulasiraman, V. Failures in stainless steel orthopaedic implant devices: A survey. *J. Mater. Sci. Lett.* **1995**, *14*, 351–354. [CrossRef]
15. Beddoes, J.; Bucci, K. The influence of surface condition on the localized corrosion of 316L stainless steel orthopaedic implants. *J. Mater. Sci. Mater. Med.* **1999**, *10*, 389–394. [CrossRef]
16. Asri, R.I.M.; Harun, W.S.W.; Samykano, M.; Lah, N.A.C.; Ghani, S.A.C.; Tarlochan, F.; Raza, M.R. Corrosion and surface modification on biocompatible metals: A review. *Mater. Sci. Eng. C* **2017**, *77*, 1261–1274. [CrossRef]
17. Finšgar, M.; Uzunalić, A.P.; Stergar, J.; Gradišnik, L.; Maver, U. Novel chitosan/diclofenac coatings on medical grade stainless steel for hip replacement applications. *Sci. Rep.* **2016**, *6*, 26653. [CrossRef]

18. Bayón, R.; Igartua, A.; González, J.J.; De Gopegui, U.R. Influence of the carbon content on the corrosion and tribocorrosion performance of Ti-DLC coatings for biomedical alloys. *Tribol. Int.* **2015**, *88*, 115–125. [CrossRef]
19. Fojt, J.; Joska, L.; Málek, J. Corrosion behaviour of porous Ti–39Nb alloy for biomedical applications. *Corros. Sci.* **2013**, *71*, 78–83. [CrossRef]
20. Cordeiro, J.M.; Beline, T.; Ribeiro, A.L.R.; Rangel, E.C.; da Cruz, N.C.; Landers, R.; Faverani, L.P.; Vaz, L.G.; Fais, L.M.; Vicente, F.B.; et al. Development of binary and ternary titanium alloys for dental implants. *Dent. Mater.* **2017**, *33*, 1244–1257. [CrossRef]
21. Mjöberg, B.; Hellquist, E.; Mallmin, H.; Lindh, U. Aluminum, Alzheimer's disease and bone fragility. *Acta Orthop. Scand.* **1997**, *68*, 511–514. [CrossRef]
22. Mirza, A.; King, A.; Troakes, C.; Exley, C. Aluminium in brain tissue in familial Alzheimer's disease. *J. Trace Elem. Med. Biol.* **2017**, *40*, 30–36. [CrossRef]
23. Chen, Q.; Thouas, G.A. Metallic implant biomaterials. *Mater. Sci. Eng. R Rep.* **2015**, *87*, 1–57. [CrossRef]
24. Singh, R.; Dahotre, N.B. Corrosion degradation and prevention by surface modification of biometallic materials. *J. Mater. Sci. Mater. Med.* **2007**, *18*, 725–751. [CrossRef]
25. Manam, N.S.; Harun, W.S.W.; Shri, D.N.A.; Ghani, S.A.C.; Kurniawan, T.; Ismail, M.H.; Ibrahim, M.H.I. Study of corrosion in biocompatible metals for implants: A review. *J. Alloy. Compd.* **2017**, *701*, 698–715. [CrossRef]
26. Wang, X.; Li, Y.; Xiong, J.; Hodgson, P.D.; Wen, C.E. Porous TiNbZr alloy scaffolds for biomedical applications. *Acta Biomater.* **2009**, *5*, 3616–3624. [CrossRef]
27. Ramírez, G.; Rodil, S.E.; Arzate, H.; Muhl, S.; Olaya, J.J. Niobium based coatings for dental implants. *Appl. Surf. Sci.* **2011**, *257*, 2555–2559. [CrossRef]
28. Reyes, K.M.; Kuromoto, N.K.; Claro, A.A.; Marino, C.E.B. Electrochemical stability of binary TiNb for biomedical applications. *Mater. Res. Express* **2017**, *4*, 075402. [CrossRef]
29. Kapnisis, K.; Constantinou, M.; Kyrkou, M.; Nikolaou, P.; Anayiotos, A.; Constantinides, G. Nanotribological response of aC: H coated metallic biomaterials: The cases of stainless steel, titanium, and niobium. *J. Appl. Biomater. Funct. Mater.* **2018**, *16*, 230–240.
30. Ou, K.L.; Weng, C.C.; Lin, Y.H.; Huang, M.S. A promising of alloying modified beta-type Titanium-Niobium implant for biomedical applications: Microstructural characteristics, in vitro biocompatibility and antibacterial performance. *J. Alloy. Compd.* **2017**, *697*, 231–238. [CrossRef]
31. Tavares, A.M.G.; Fernandes, B.S.; Souza, S.A.; Batista, W.W.; Cunha, F.G.C.; Landers, R.; Macedo, M.C.S.S. The addition of Si to the Ti–35Nb alloy and its effect on the corrosion resistance, when applied to biomedical materials. *J. Alloy. Compd.* **2014**, *591*, 91–99. [CrossRef]
32. Lee, C.; Ju, C.-P.; Chern Lin, J. Structure–property relationship of cast Ti–Nb alloys. *J. Oral Rehab.* **2002**, *29*, 314–322. [CrossRef]
33. Gabriel, S.B.; Panaino, J.V.P.; Santos, I.D.; Araujo, L.S.; Mei, P.R.; De Almeida, L.H.; Nunes, C.A. Characterization of a new beta titanium alloy, Ti–12Mo–3Nb, for biomedical applications. *J. Alloy. Compd.* **2012**, *536*, S208–S210. [CrossRef]
34. Ali, S.; Rani, A.M.A.; Altaf, K.; Hussain, P.; Prakash, C.; Hastuty, S.; Rao, T.V.V.L.N.; Subramaniam, K. Investigation of alloy composition and sintering parameters on the corrosion resistance and microhardness of 316L Stainless Steel alloy. In *Advances in Manufacturing II*; Gapiński, B., Szostak, M., Ivanov, V., Eds.; Springer: Berlin, Germany, 2019; pp. 532–541.
35. Bagliuk, G. Properties and structure of sintered boron containing carbon steels. In *Sintering-Methods and Products*; Shatokha, V., Ed.; IntechOpen: London, UK, 2012.
36. Bayraktaroglu, E.; Gulsoy, H.O.; Gulsoy, N.; Er, O.; Kilic, H. Effect of boron addition on injection molded 316L stainless steel: Mechanical, corrosion properties and in vitro bioactivity. *Bio Med. Mater. Eng.* **2012**, *22*, 333–349.
37. Kurgan, N. Effects of sintering atmosphere on microstructure and mechanical property of sintered powder metallurgy 316L stainless steel. *Mater. Des. (1980–2015)* **2013**, *52*, 995–998. [CrossRef]
38. Ali, S.; Rani, A.; Majdi, A.; Mufti, R.A.; Hastuty, S.; Hussain, M.; Shehzad, N.; Baig, Z.; Aliyu, A.; Azeez, A. An Efficient Approach for Nitrogen Diffusion and Surface Nitriding of Boron-Titanium Modified Stainless Steel Alloy for Biomedical Applications. *Metals* **2019**, *9*, 755. [CrossRef]
39. Chao, Z.; Yaomu, X.; Chufeng, L.; Conghua, L. The effect of mucin, fibrinogen and IgG on the corrosion behaviour of Ni–Ti alloy and stainless steel. *Biometals* **2017**, *30*, 367–377. [CrossRef]

40. Hussein, M.A.; Yilbas, B.; Kumar, A.M.; Drew, R.; Al-Aqeeli, N. Influence of Laser Nitriding on the Surface and Corrosion Properties of Ti-20Nb-13Zr Alloy in Artificial Saliva for Dental Applications. *J. Mater. Eng. Perform.* **2018**, *27*, 4655–4664. [CrossRef]
41. Nassar, A.E.; Nassar, E.E. Properties of aluminum matrix Nano composites prepared by powder metallurgy processing. *J. King Saud Univ. Eng. Sci.* **2017**, *29*, 295–299. [CrossRef]
42. Čapek, J.; Stehlíková, K.; Michalcová, A.; Msallamová, Š.; Vojtěch, D. Microstructure, mechanical and corrosion properties of biodegradable powder metallurgical Fe-2 wt % X (X= Pd, Ag and C) alloys. *Mater. Chem. Phys.* **2016**, *181*, 501–511. [CrossRef]
43. Singh, A.V.; Jahnke, T.; Xiao, Y.; Wang, S.; Yu, Y.; David, H.; Richter, G.; Laux, P.; Luch, A.; Srivastava, A.; et al. Peptide-Induced Biomineralization of Tin Oxide (SnO_2) Nanoparticles for Antibacterial Applications. *J. Nanosci. Nanotech.* **2019**, *19*, 5674–5686. [CrossRef]
44. Bauer, S.; Schmuki, P.; Von Der Mark, K.; Park, J. Engineering biocompatible implant surfaces: Part I: Materials and surfaces. *Prog. Mater. Sci.* **2013**, *58*, 261–326. [CrossRef]